HAL
open science

Slow motions in A×T rich DNA sequence

A Ben Imeddourene, L Zargarian, M Buckle, B Hartmann, Olivier Mauffret

To cite this version:

A Ben Imeddourene, L Zargarian, M Buckle, B Hartmann, Olivier Mauffret. Slow motions in A×T rich DNA sequence. Scientific Reports, 2020, 10, 10.1038/s41598-020-75645-x . hal-03430851

HAL Id: hal-03430851

https://hal.science/hal-03430851v1

Submitted on 16 Nov 2021

HAL is a multi-disciplinary open access archive for the deposit and dissemination of scientific research documents, whether they are published or not. The documents may come from teaching and research institutions in France or abroad, or from public or private research centers.

L'archive ouverte pluridisciplinaire **HAL**, est destinée au dépôt et à la diffusion de documents scientifiques de niveau recherche, publiés ou non, émanant des établissements d'enseignement et de recherche français ou étrangers, des laboratoires publics ou privés.

scientific reports

Check for updates

OPEN

Slow motions in A·T rich DNA sequence

A. Ben Imeddourene, L. Zargarian, M. Buckle, B. Hartmann & O. Mauffret✉

In free B-DNA, slow (microsecond-to-millisecond) motions that involve equilibrium between Watson–Crick (WC) and Hoogsteen (HG) base-pairing expand the DNA dynamic repertoire that could mediate DNA–protein assemblies. $R_{1\rho}$ relaxation dispersion NMR methods are powerful tools to capture such slow conformational exchanges in solution using $^{13}C/^{15}N$ labelled DNA. Here, these approaches were applied to a dodecamer containing a TTAAA element that was assumed to facilitate nucleosome formation. NMR data and inferred exchange parameters assign HG base pairs as the minor, transient conformers specifically observed in three successive A·T base pairs forming the TAA·TTA segment. The abundance of these HG A·T base pairs can be up to 1.2% which is high compared to what has previously been observed. Data analyses support a scenario in which the three adenines undergo non-simultaneous motions despite their spatial proximity, thus optimising the probability of having one HG base pair in the TAA·TTA segment. Finally, revisiting previous NMR data on H2 resonance linewidths on the basis of our results promotes the idea of there being a special propensity of A·T base pairs in TAA·TTA tracts to adopt HG pairing. In summary, this study provides an example of a DNA functional element submitted to slow conformational exchange. More generally, it strengthens the importance of the role of the DNA sequence in modulating its dynamics, over a nano- to milli-second time scale.

DNA–protein recognition processes occur through so-called direct and indirect readout of DNA by proteins. The formation of nucleoprotein complexes requires in particular, recognition of DNA chemical patterns specific to each base, and DNA structural and dynamic features that are sequence dependent. Deciphering the dynamics of DNA is not experimentally easy. Nuclear Magnetic Resonance (NMR) has long been, and remains a powerful technique for capturing picosecond dynamics at atomic resolution; more recent developments of relaxation dispersion experiments extend the timescale up to milliseconds and quantitatively investigate slow conformational exchange processes[1–4].

Initially, the existence of slow dynamic movements in DNA emerged from early NMR data collected on adenines of TpA steps, by detecting an excess linewidth of adenine H2-resonance protons in biologically active DNA sequences[5,6]. Further investigations showed that this linewidth broadening was sensitive to the TpA tetranucleotide sequence context[6–8]. The observation of these resonance experiments was interpreted as being due to a slow exchange between two conformational states[7,9,10], which could arise because of poor TpA stacking[9,10].

$R_{1\rho}$ relaxation dispersion NMR experiments have led to major advances in this field. These experiments were used to reveal and characterize slow conformational equilibria between major and minor conformational states, assimilated to ground and excited states in analogy with spectroscopy. The use of double ^{13}C and ^{15}N labelled molecules allowed the detection and analysis of excited conformer populations of less than 1%. This approach initially provided insights on various topics essentially related to proteins such as folding, enzymatic catalysis, ligand binding and recognition[1,2,11], but now also gives information about intrinsic slow motions of nucleic acids[3,12–16]. Applied to B-DNA double helices, this methodology revealed an unexpected equilibrium between two schemes of base-pairing: standard Watson–Crick (WC) base pairs being able to transiently adopt the Hoogsteen (HG) configuration[15,17–20]. Prior to these NMR studies, the first experimental evidence of HG pairing in DNA was obtained in 2002 using a DNA containing 6 A·T base pairs that all crystallized in the HG mode[21]. Both experimental[22] and theoretical[23] approaches showed that $d(AT)_n$ sequences were globally more stable in the classical WC B-DNA than in a fully HG double helix, at least in dilute aqueous solutions and in the absence of cofactors. However, earlier models[24] as well as more sophisticated MD structures[15,25,26] demonstrated that HG pairing can coexist with WC base pairs in the same DNA without generating prohibitive energy cost. Thus, the presence of transient HG base pairs in solution, as shown by NMR, is strongly supported by these previous reports.

LBPA, ENS de Paris-Saclay, UMR 8113 CNRS, Institut D'Alembert, Université Paris-Saclay, 4, avenue des Sciences, 91190 Gif-sur-Yvette, France. ✉email: olivier.mauffret@ens-paris-saclay.fr

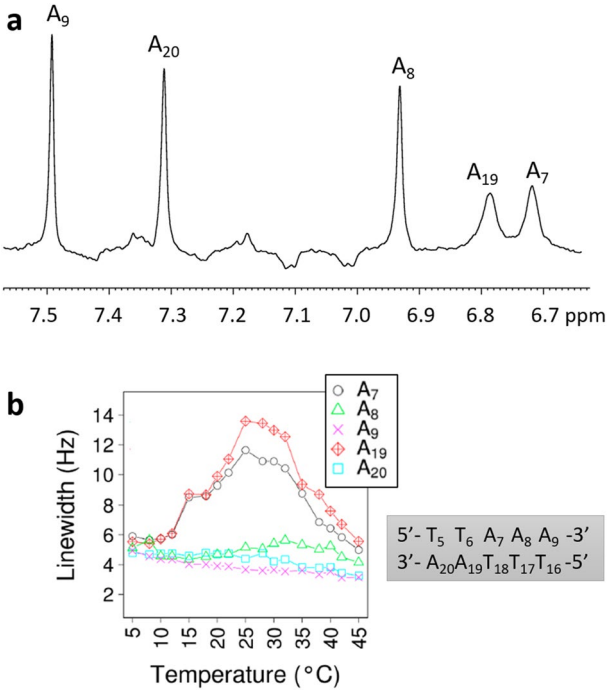

Figure 1. Chemical shifts and linewidth of H2 adenine proton resonances. (**a**) 1D-T1 inversion recovery spectrum of the aromatic region of the unlabelled oligomer at 25 °C in ^2H_2O, after having selected the inversion recovery delay to only obtain the H2 resonances of adenines. (**b**) Linewidths (measured at half-width) of H2 adenine proton resonances as a function of temperature. The numbering of the DNA segment of interest is given on the right of the Figure.

Relaxation dispersion NMR studies provided quantitative information that covered three different aspects of the WC↔HG exchange process, thermodynamic (conformer populations), kinetic (exchange rates) and structural (chemical shifts of the minor conformer). Modulation of this equilibrium by the base pair type (A·T *versus* G·C) and the sequence surrounding the base pair[15,17,27] was established, in agreement with, and as a complement to, analyses of H2-linewidth broadening.

That HG or HG-like T·A in TpA steps are found relatively frequently in X-ray structures of DNA duplexes suggests a biological role for the WC↔HG equilibrium[27]. In addition to their possible involvement through base-pairing, TpA steps also play a role in nucleoprotein complexes as illustrated by the case of nucleosomes whose positioning along eukaryotic genomes is biased by the DNA sequence. Thus, favourable sequences for forming nucleosomes in vivo as well as in vitro are composed in such a way that A·T-rich and G·C-rich minor grooves generally tend to face towards and away from the histone core, respectively[28–32]. This is particularly the case for the 601 sequence, also called the "Widom sequence", which is widely used for positioning nucleosomes because of its high affinity for the histone octamer[33], further enhanced by an enrichment of additional strategically located TpA steps[34–37]. To better understand the properties of the 601 sequence we carried out classic NMR experiments[37] and modelling[38] studying four dodecamers that together cover 39 base pairs of the 5′ half of the 601 sequence. One of these dodecamers contains the TTAAA fragment that, in its ground state, shows a remarkable narrowing of its minor groove[37]. This structural characteristic is thought to be associated with an enhanced electronegative potential[39] that is especially attractive for the histone arginines anchoring the DNA. Given the above, we decided to further extend the exploration of the properties of the dodecamer whose sequence and numbering is given below:

5′- C_1 C_2 G_3 C_4 $\underline{\mathbf{T_5}}$ $\underline{\mathbf{T_6}}$ $\underline{\mathbf{A_7}}$ $\underline{\mathbf{A_8}}$ $\underline{\mathbf{A_9}}$ $C_{10}G_{11}C_{12}$ -3′

3′- $G_{24}G_{23}C_{22}G_{21}\underline{\mathbf{A_{20}}}\underline{\mathbf{A_{19}}}\underline{\mathbf{T_{18}}}\underline{\mathbf{T_{17}}}\underline{\mathbf{T_{16}}}G_{15}C_{14}G_{13}$ -5′

Here, we will describe NMR experiments, in particular $R_{1\rho}$ relaxation dispersion experiments, that were used to study this dodecamer. Careful analysis and interpretation of the NMR data led to the detection and characterization of slow motions on a patch of 3 successive A·T base pairs in TpA·TpA and ApA·TpT contexts, which participate in WC↔HG equilibria. These findings were put into perspective with regard to previous studies in order to discuss the sequence effect on slow motion.

Results

1D spectra of H2 protons. In 1D (Supplementary Fig. S1) and 1D-T1 inversion-recovery (Fig. 1a) spectra, the five H2 protons of A_7, A_8, A_9, A_{19} and A_{20} show a very large spectral dispersion compared to those of other non-exchangeable protons. Such dispersion is expected because H2 chemical shifts are extremely sensitive to their sequence environment[6–8], notably with high-field shifts specific to TpA adenines[9,10].

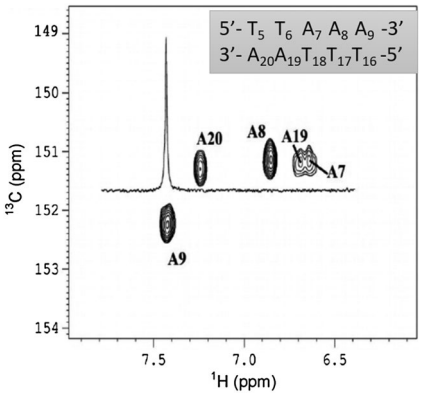

Figure 2. H2–C2 region of adenines of a constant-time HSQC spectrum. The H2–C2 region of adenines of a ^{13}C–^{1}H constant-time HSQC spectrum (600 MHz) was obtained on the labelled oligomer at 25 °C. The ^{1}H 1D spectrum was superposed on the proton frequencies from 1D ^{13}C $R_{1\rho}$ dispersion experiment at the ^{1}H and ^{13}C frequency of A_9 signal.

Here, the H2 chemical shifts of A_7 and A_{19} are in fact strongly high-field shifted (Fig. 1a) in the unique $TpA_7{\cdot}TpA_{19}$ complementary dinucleotide of the studied dodecamer (see the sequence in above "Introduction" section). Although these adenines share the same tetranucleotide context ($TTA_7A{\cdot}TTA_{19}A$), their H2 chemical shifts are clearly different (Fig. 1a). Thus, the sensitivity of H2 chemical shifts to the sequence depends on both 5′ and 3′ nearest neighbours and not only on the 3′ base as previously postulated[10,40].

A key point is that the H2 resonances of A_7 and A_{19} are severely broadened compared to those of A_8, A_9 and A_{20} (Fig. 1a). These A_7 and A_{19} H2 broadenings are detected below the Tm of 57 °C (Supplementary Fig. S2) and their amplitudes are maximal between 25 and 30 °C (Fig. 1b). Such behaviour of H2 adenine resonances resembles other TpA results that were interpreted as being the signature for conformational motion[5–9] occurring at the microsecond-millisecond range[41].

C2–H2 cross-peaks were then identified from a constant-time ^{1}H–^{13}C spectrum. Weak intensity and significant broadenings are observed for only A_{19} and A_7 cross-peaks. 1D H2 inversion-recovery and 1D dispersion R1ρ relaxation spectra show that both H2 and C2 resonances of A_{19} and A_7 are involved in these specific cross-peak particularities. So, the motions detected here influence the NMR behaviour of at least these two adenine atoms.

The next step was to apply $R_{1\rho}$ relaxation dispersion experiments to the $^{13}C/^{15}N$ labelled dodecamer, as a means to follow and describe slow conformational exchanges. The 1D selective $R_{1\rho}$ spectrum of the A_9 resonance illustrates the good selectivity of this type of experiment, ensuring that the excitation of a given carbon does not affect its spectrum neighbours (Fig. 2).

On-resonance ^{13}C $R_{1\rho}$ dispersion relaxation experiments: evidence of slow conformational exchanges. $R_{1\rho}$ relaxation dispersion experiments[14] in the on-resonance version constituted a first approach for identifying those carbon atoms of nucleotides submitted to slow conformational exchange. The $R_{1\rho}$ rates were carefully measured to obtain the best estimate of the exponential decreasing ^{13}C magnetization. Typical plots of mono-exponential decays of the type shown in Supplementary Fig. S3 illustrate the quality of the data. The $R_{1\rho}$ profiles measured as a function of effective spin-lock field power were fitted using a two-state model and two variables, the relaxation rate R_2 and the exchange rate R_{ex} (see "Materials and Methods"); 500 runs were performed per fit, to obtain R_2 and R_{ex} standard deviations.

C2 atoms of adenines. The C2 atoms of A_7, A_8, A_9, A_{19} and A_{20} (Fig. 3) were studied first. Evidence of a slow conformational exchange on A_7 and A_{19} emerges from the profiles of their $R_{1\rho}$ ($=R_2+R_{ex}$) rates measured as a function of effective spin-lock field power (Fig. 3). These profiles and their fits show that C2-R_{ex} is higher for A_{19} than for A_7 (Fig. 3 and Supplementary Table S2-1 for both R_2 and R_{ex} values). The consistency between these results and those obtained on H2 adenine atoms (Figs. 1 and 2) argues in favour of a major effect of slow motion on H2 and C2 linewidths. The on-resonance data collected on A_8, A_9 and A_{20} C2 atoms reveal invariant $R_{1\rho}$ values (Fig. 3) and thus null R_{ex} values (Supplementary Table S2-1).

C6 or C8 atoms. The C6/C8 on-resonance NMR signals were resolved for over half of the dodecamer nucleotides, comprising A_9, but severe spectral overlaps occurred for several residues, preventing in particular the distinction of A_7 from A_{19}, and A_9 from A_{20}. The fitting R_2 and R_{ex} values for the profiles of $R_{1\rho}$ rates as a function of effective spin-lock field power are given in Supplementary Table S2-2. Thus, the existence of a conformational exchange is attested for A_7 and/or A_{19}, A_9 and/or A_{20}, and A_8 (Fig. 4), with R_{ex} values similar to the highest ones obtained on previous DNA slow motion studies performed in appropriate pH and temperature conditions[15,17,18]. Such events are excluded or at least much more questionable for the remaining nucleotides that display flat $R_{1\rho}$ profiles (examples in Supplementary Fig. S4) and therefore null or low R_{ex} values (<2.3 Hz) (Supplementary Table S2-2).

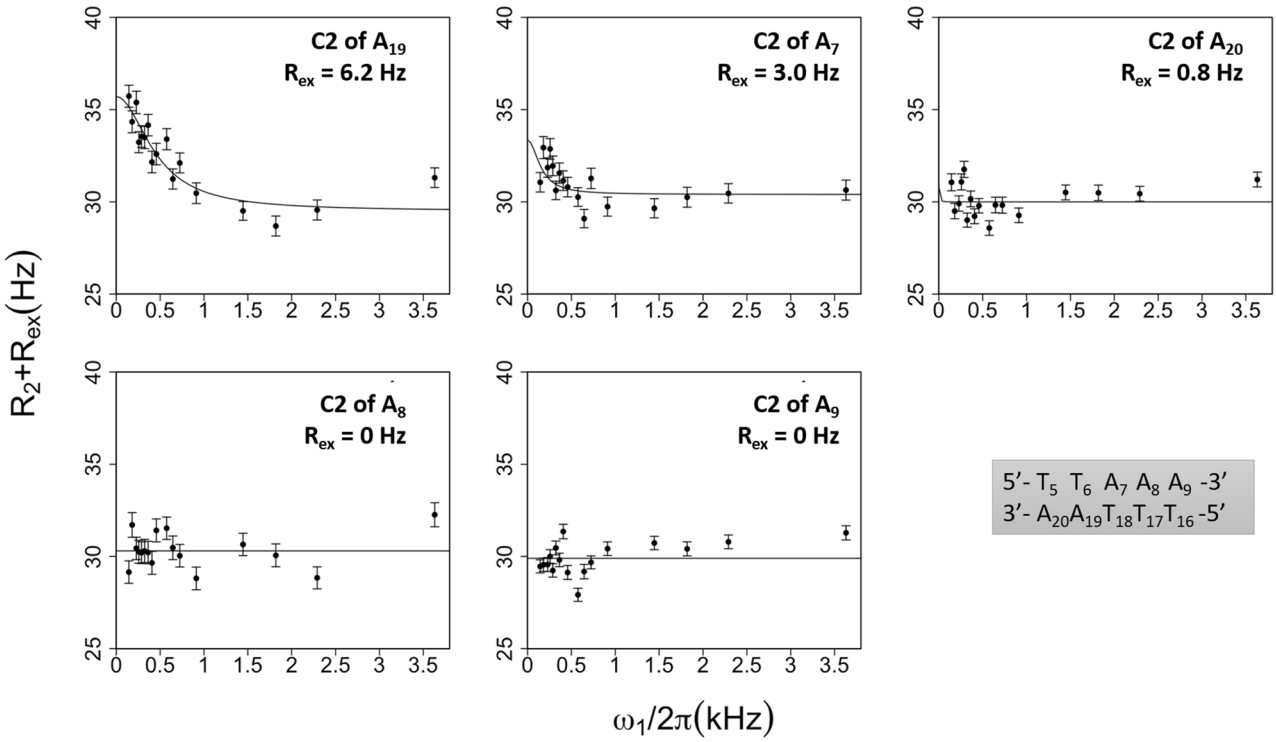

Figure 3. On-resonance $R_{1\rho}$ relaxation dispersion profiles of C2 atoms of adenines. $R_{1\rho}$ ($=R_2+R_{ex}$) rates of the C2 atoms of the five adenines were plotted as a function of the effective spin-lock field power ($\omega 1/2\pi$). The experiments were performed at 25 °C. The two-state model fits (solid lines) were obtained using the protocol described in "Materials and Methods"; (R_2+R_{ex}) standard deviations were calculated from the 500 runs carried out for each fit. The averaged R_{ex} values are specified in each panel. Top: $R_{ex}>0$; bottom: $R_{ex}\sim 0$.

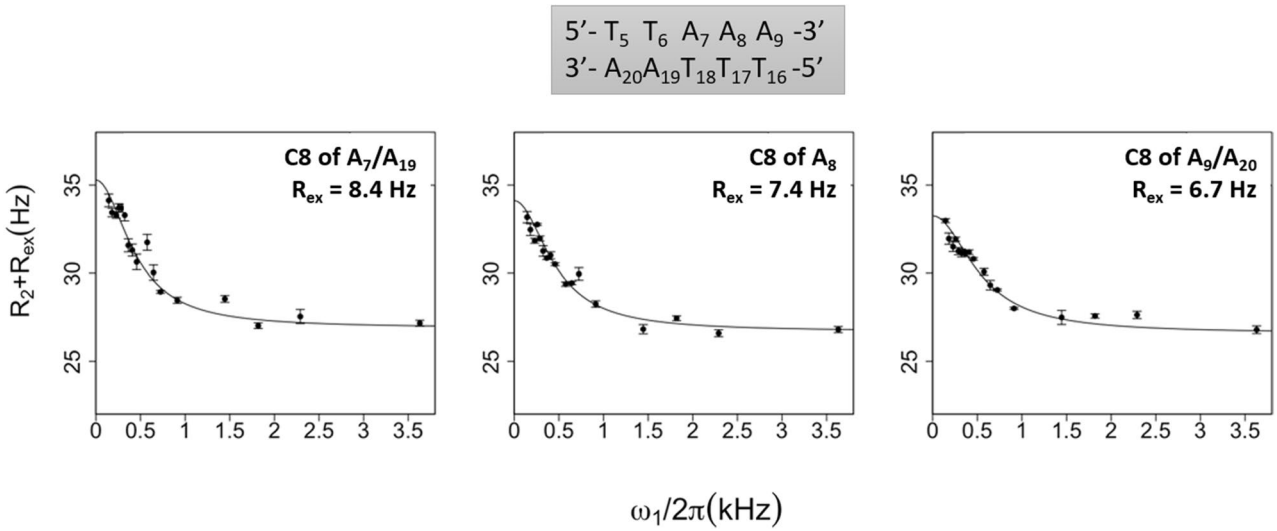

Figure 4. On-resonance $R_{1\rho}$ relaxation dispersion profiles of adenine C8 atoms. $R_{1\rho}$ ($=R_2+R_{ex}$) rates of the C8 atoms of adenines were plotted as a function of the effective spin-lock field power ($\omega 1/2\pi$). The experiments were performed at 25 °C. The two-state model fits (solid lines) were obtained using the protocol described in "Materials and Methods". (R_2+R_{ex}) standard deviations were calculated from the 500 runs carried out for each fit. The averaged R_{ex} values are specified in each panel.

C1′ atoms. A third series of experiments was carried out on the anomeric C1′ atoms. The (R_2+R_{ex}) profiles (Fig. 5) and the R_2 and R_{ex} values (Fig. 5 and Supplementary Table S2-3) show that the data related to the C1′ atoms of A_7, A_8, A_9 and A_{19} are compatible with a slow conformational equilibrium. Among these four adenines, A_7 and A_{19} are associated with especially high R_{ex} values (>15 Hz) that exceed available measurements[15,17] and reflect a relative abundance of excited state[3]. The flat $R_{1\rho}$ profiles obtained for the C1′ atoms of other nucleo-

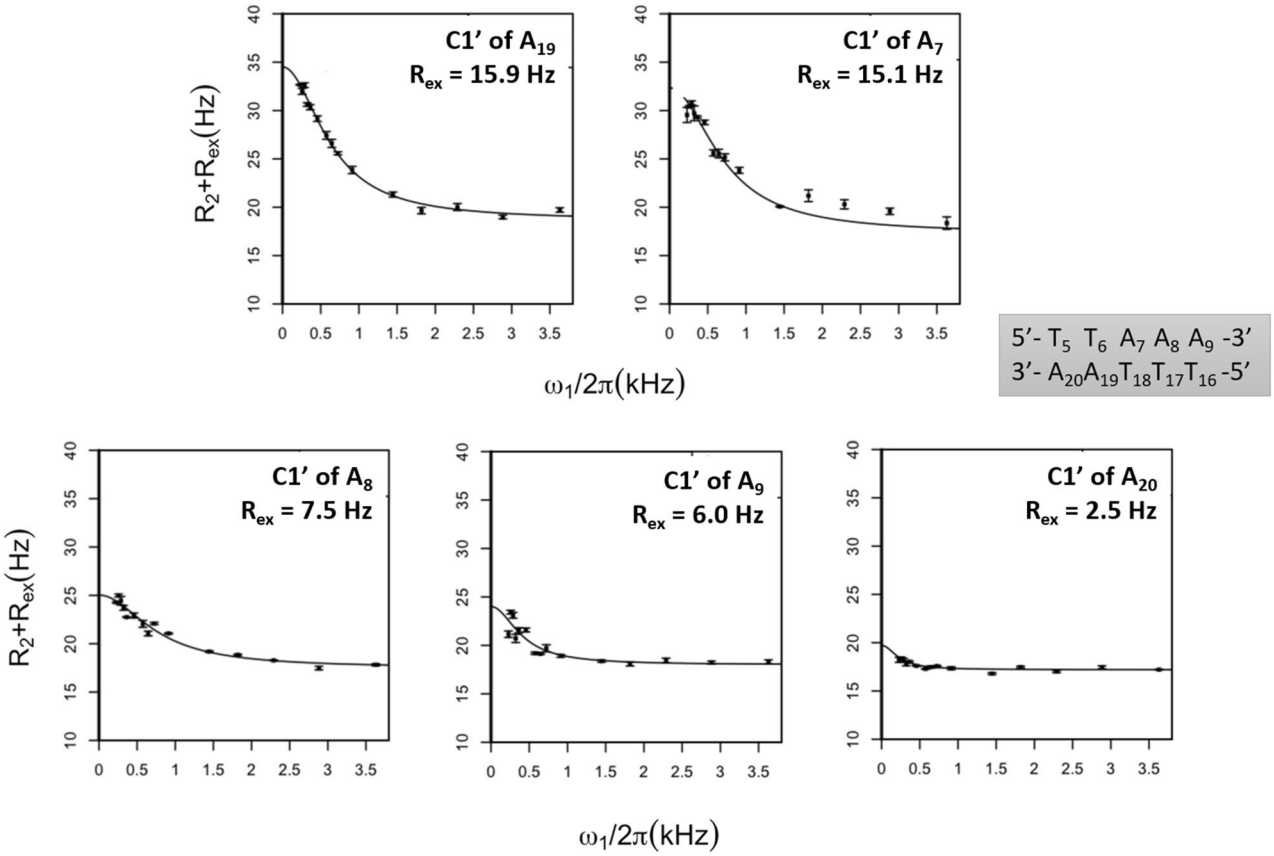

Figure 5. On-resonance $R_{1\rho}$ relaxation dispersion profiles of adenines C1′ atoms. $R_{1\rho}$ ($=R_2+R_{ex}$) rates of the C1′ atoms of adenines were plotted as a function of the effective spin-lock field power ($\omega 1/2\pi$). The experiments were performed at 25 °C. The two-state model fits (solid lines) were obtained using the protocol described in "Materials and Methods". (R_2+R_{ex}) standard deviations were calculated from the 500 runs carried out for each fit. The averaged R_{ex} values are specified in each panel.

Atom type	High R_{ex} value	Low R_{ex} value
C2	$R_{ex} \geq 2.5\ s^{-1}$: A_7 A_{19}	–
C8	$R_{ex} \geq 6.7\ s^{-1}$: (A_7 and/or A_{19}) A_8 (A_9 and/or A_{20})	–
C1'	$R_{ex} \geq 6.0\ s^{-1}$: A_7 A_8 A_9 A_{19}	$R_{ex} \leq 2.5\ s^{-1}$: A_{20}

Table 1. Adenines in $T_5T_6A_7A_8A_9{\cdot}T_{16}T_{17}T_{18}A_{19}A_{20}$ associated with non-null R_{ex} value according to on-resonance relaxation dispersion experiments.

tides, comprising thymine partners of adenines, correspond to much lower or null R_{ex} values (Supplementary Table S2-3).

When C1′ and C6–C8 relaxation dispersion experiments are available for the same nucleotide, R_2 and R_{ex} values are consistent (Supplementary Table S2-2 vs Supplementary Table S2-3). Assuming that this property is true for all the nucleotides, the present relaxation dispersion experiments help to interpret the data subject to C8 atom resonance overlaps which concern in particular the nucleotide couples A_7/A_{19} and A_9/A_{20} (Fig. 4). Thus, both A_7 and A_{19} likely contribute to C8 relaxation dispersion; the R_{ex} values, clearly higher for C1′ of A_9 than for C1′ of A_{20}, advocate for a major contribution of A_9 to C8-R_{ex}.

In sum. Null R_{ex} values show that there is no slow exchange on C·G base pairs, which is the norm at our pH conditions (pH 6.5)[42]. Also, the R_{ex} values calculated for the thymines paired with the five adenines do not furnish any robust evidence for motions (Supplementary Table S2). In contrast, non-null R_{ex} values appear on the five dodecamer adenines (Table 1). It is clear that A_7 and A_{19} in $T_6pA_7{\cdot}T_{18}pA_{19}$ are submitted to a slow conformational equilibrium, according to consistent, high R_{ex} values from C2, C8 and C1′ on-resonance experiments and to H2 and C2 linewidth broadenings. Among the three neighbouring adenines, A_8 and A_9 exhibit signs of dynamic events although the behaviour of their H2 and C2 atoms differ from those of A_7 and A_{19}; the case of A_{20} is much more disputable, given the low R_{ex} value associated with its C1′ atom.

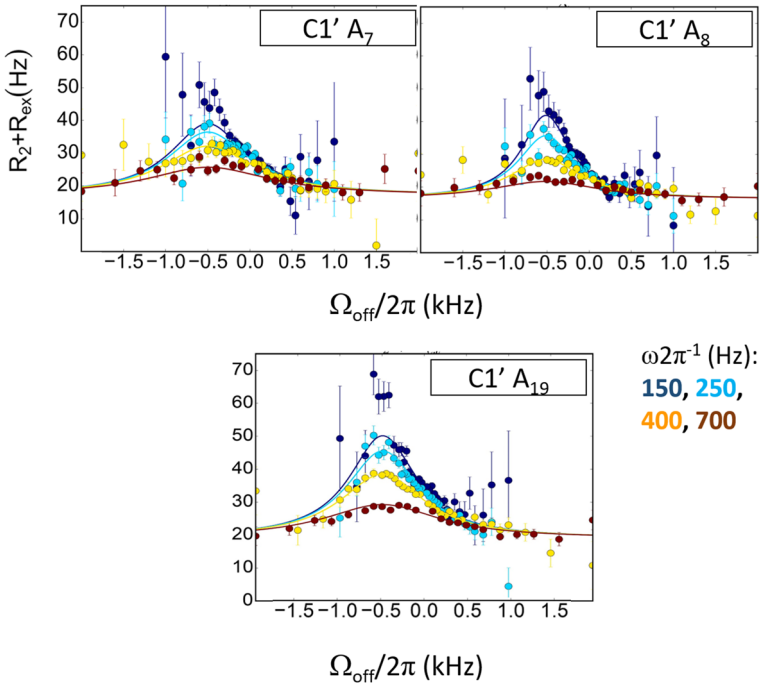

Figure 6. Off-resonance $R_{1\rho}$ relaxation dispersion profiles for C1′ atoms of A_7, A_8 and A_{19}. $R_2 + Rex$ ($= R_{1\rho}$) values are given as a function of the resonance offset from the major state ($\Omega_{off}/2\pi$). Error bars represent experimental uncertainties. The experiments were carried out at four different spin-lock powers (From 150 to 700 Hz, colour code given in the bottom right of the Figure). The fits (solid lines) were performed using Method 2, described in "Materials and Methods". The resulting exchange parameters are reported in Tables 2 and S3.

On-resonance experiments are commonly used to provide information about the presence or absence of slow motion but by themselves they are insufficiently accurate for a viable quantification of the exchange parameters. Consequently, more sophisticated off-resonance experiments were also carried out to extract significant information about the conformational exchange process.

Off-resonance $R_{1\rho}$ dispersion relaxation experiments: characteristics of slow conformational exchange. Off-resonance dispersion relaxation experiments performed at a single magnetic field were used to obtain thermodynamic, kinetic and structural information about conformational exchange. This type of experiment was applied to the C1′ resonances of A_7, A_8, A_9 and A_{19}; the four adenines for which signs of exchange arise from on-resonance dispersion relaxation experiments. Additional investigations focused on T_6, C_4, G_{15} and G_{21}, nucleotides associated to very low or null R_{ex} (Supplementary Table S2). C1′ resonances were chosen because they showed large signal to noise ratios and were subject to only a few overlaps so that data could be collected for most nucleotides of the dodecamer (Supplementary Tables S2, S3).

The off-resonance data are compatible with slow motions for A_7, A_8, and A_{19} alone (Fig. 6). A_9, as well as the other nucleotides are associated with flat ($R_2 + R_{ex}$) profiles (examples in Supplementary Fig. S5). The A_7, A_8, and A_{19} ($R_2 + R_{ex}$) profiles were fitted using two distinct methods, an approach that enables to assess the robustness of the resulting parameters. We implemented first a classical analytic, algebraic method[15,43–45], described as Method 1 in "Materials and Methods", performing 1000 runs of calculations for each fit. The same data were also analysed using a completely different method recently published[3], called here Method 2, which is based on the numerical integration of the Bloch-McConnell equations. Basically, both methods rely on a two-state exchange model and three variables, the rate exchange (k_{ex}), the population of the minor conformer (p_E) and the difference between the chemical shifts of major and minor conformers ($\Delta\omega$). Examples of fits with Method 2 are given in Fig. 6.

Applied to A_7, A_8 and A_{19} data, the exchange parameters from either Methods 1 or 2 are remarkably consistent (Tables 2 and S3), in the range of those previously published[15,17–20]. The rather modest standard deviations associated with the parameter values from Method 1 show the reliability of each run series. Nevertheless, some subtle differences are observed for the A_7 exchange obtained from the two methods. Although it is clear that this nucleotide is submitted to a slow exchange, the A_7-$\Delta\omega$ value and standard deviation (4.16 ± 1.06 ppm) obtained from Method 1 appear too high compared to published data[15,17–20]. In addition, one expects a substantial p_E value, similar to that of A_{19}, given their comparable high R_{ex} values that are primarily sensitive to the excited state population[3]. For these reasons, we prefer to give more weight to the A_7-parameters from Method 2.

The data related to A_7 and A_{19} strengthen the interpretation of H2 and C2 linewidth broadening proposed above from on-resonance results. Indeed, there is now a clear parallel between H2 and C2 broadenings (Figs. 1 and 2), R_{ex} values (Fig. 3) and p_E (Table 2), all of these parameters being more accentuated for A_{19} than for A_7.

C1′ nucleotide	k_{ex} (s^{-1})		p_E (%)		Δω (ppm)	
	Method 1	Method 2	Method 1	Method 2	Method 1	Method 2
A_7	2991 ± 693	3309 ± 357	0.62 ± 0.19	0.80 ± 0.08	4.16 ± 1.06	3.32 ± 0.16
A_8	1580 ± 306	1994 ± 199	0.58 ± 0.09	0.59 ± 0.02	3.53 ± 0.51	3.42 ± 0.1
A_{19}	2680 ± 456	2872 ± 205	1.20 ± 0.01	1.00 ± 0.05	3.31 ± 0.32	3.29 ± 0.09

Table 2. A_7, A_8 and A_{19} conformational exchange parameters from C1′ off-resonance $R_{1\rho}$ relaxation dispersion experiments. The exchange parameters presented in this Table correspond to the population of the minor conformer (p_E), the rate exchange (k_{ex}) and the difference between the chemical shifts of major and minor conformers (Δω); they were inferred from individual fits of C1′ off-resonance relaxation dispersion data according to a classical, home-made protocol (Method 1, see "Materials and Methods") or an approach developed by Al Hashimi's group (Method 2). Experimental data were collected at 600 MHz, 25 °C and pH 6.5.

A_{19} atom(s)	k_{ex} (s^{-1})		p_E (%)		Δω (ppm) for C1'	
	Method 1	Method 2	Method 1	Method 2	Method 1	Method 2
C1′ alone	2680 ± 456	2872 ± 205	1.20 ± 0.01	1.00 ± 0.05	3.31 ± 0.32	3.29 ± 0.09
C1′, C8, C2 together	2671 ± 459	3138 ± 228	1.20 ± 0.20	1.10 ± 0.08	3.31 ± 0.31	3.31 ± 0.09

Table 3. A_{19} conformational exchange parameters from off-resonance $R_{1\rho}$ relaxation dispersion experiments. The exchange parameters presented in this Table correspond to the population of the minor conformer (p_E), the rate exchange (k_{ex}) and the difference between the chemical shifts of major and minor conformers (Δω); they were inferred from fits of off-resonance relaxation dispersion data according to Methods 1 or 2; the data are those collected from resonances of either C1′ alone or C1′, C8 and C2 together, at 600 MHz, 25 °C and pH 6.5.

	k_{ex} (s^{-1})		p_E (%)		Δω (ppm)	
	Method 1	Method 2	Method 1	Method 2	Method 1	Method 2
C1′ of A_7, A_8 and A_{19}	2391 ± 299	2678 ± 153	0.85 ± 0.53	0.85 ± 0.11	3.32 ± 0.43	2.83 ± 0.11
					3.09 ± 0.33	2.59 ± 0.07
					3.71 ± 0.26	3.70 ± 0.09

Table 4. Conformational exchange parameters from off-resonance $R_{1\rho}$ relaxation dispersion experiments: model of coordinated motions of A_7, A_8 and A_{19}. The exchange parameters presented in this Table were produced by fitting a model in which the three nucleotides undergo coordinated motions; this hypothesis implies identical k_{ex} and p_E for the three nucleotides.

We therefore postulate that H2 and C2 broadenings not only reveal slow motions, but are also correlated with the excited state population. We will see below that this conclusion is very pertinent in the reconsideration of the results of previous 1D NMR experiments.

The case of A_9 is intriguing and deserves a short comment. The R_{ex} profiles are either incompatible (off-resonance experiments, Supplementary Fig. S5) or compatible (on-resonance experiments, Fig. 5) with a conformational exchange. This unexpected situation has already been encountered[46] and may correspond to a scenario in which the typical limits of slow exchange are no longer valid; in particular, A_9 exchange rate could be faster than those of A_7, A_8 or A_{19}.

The results above were obtained with NMR datasets from only C1′ sugar resonances. Because of numerous resonance overlaps, off-resonance data could only be collected for C8 and C2 atoms of A_{19}, which allowed the constitution of a new extended dataset, involving sugar and base atoms. The fits of this dataset were performed assuming that C1′, C8 and C2 atoms are subjected to the same conformational exchange, with one unique value for k_{ex} and one unique value for p_E. The resulting values of k_{ex}, p_E and Δω are remarkably coherent with those obtained from C1′ resonances alone (Table 3), confirming in particular that the population of A_{19} minor conformer reaches 1.2/1.1%. From a methodological point of view, this approach shows that an off-resonance dataset from only one atom type is sufficient to produce reliable exchange parameters, with the obvious condition that the atom under consideration is implicated in the conformational transition of interest.

The similarities between the two-state exchange characteristics of A_7, A_8 and A_{19} (Table 2) could be compatible with simultaneous transitions of the three nucleotides between ground and excited states, implying the transient co-existence of three successive base pair minor conformers. Thus, we completed our analyses by testing this hypothesis of synchronous motions. A collective transition implies that k_{ex} and p_E are identical for the three nucleotides and these conditions were therefore integrated as restraints in the fit calculations. This model provides reasonable values of conformational exchange parameters (Table 4) that, at first sight, are comparable

	Degree of freedom	F-table value	F-value	p-value
Method 1	417	2.39	126	$1.7\ 10^{-70}$
Method 2			48	$2\ 10^{-33}$

Table 5. Comparison between fits assuming coordinated or uncoordinated motion models for A_7, A_8 and A_{19}. Statistical F-test using χ^2 and F-distribution analysis was performed to compare the fits based on models where A_7, A_8 and A_{19} undergo either coordinated, collective or uncoordinated, individual transitions; p-values validate the results.

to those obtained for individual motions (Table 2). Fisher tests were thus performed to evaluate which of the two hypotheses, non-simultaneous or simultaneous motions, led to the best result in terms of χ^2. With both Methods 1 and 2, the F-values largely exceed the F-table value (Table 5). In accordance with the p-values that show the statistical significance of the tests, this means without ambiguity that the model assuming individual motions of each adenine is more effective at best representing the off-resonance data.

Thus, the interpretation of the off-resonance dispersion relaxation experiments draws a picture of a block of three specific adenines that undergo slow motions between two states, the excited one representing from 0.6 to 1.2% of the conformers. While the three adenines are clustered in the $T_6A_7A_8{\cdot}T_{17}T_{18}A_{19}$ segment, they adopt a non-synchronous regime of motions.

Nature of the excited conformer. As mentioned above, both on- and off-resonance dispersion relaxation experiments and the inferred exchange parameters agree remarkably well with those obtained by Al Hashimi's group within B-DNA sequences[15,17–20]. The asymmetry of the NMR data in A·T base pairs, in which evidence of slow dynamics is observable on adenines but not on their thymine partners, is also in line with these earlier results. It is now accepted that these NMR-based characteristics correspond to a dynamic equilibrium of particular base pairs between the canonical Watson–Crick (WC) conformation and an excited, short-lived state of low abundance, which is the Hoogsteen (HG) pairing[3,15,18,19]. HG base-pairing corresponds to $N7_{purine} - N3_{pyrimidine}$ and $N6/O6_{purine} - O4/N4_{pyrimidine}$ hydrogen bonds, which imply purine and pyrimidine nucleotides in syn- and anti-configurations, respectively. Thus, the WC → HG transition does not dramatically affect the pyrimidine but requires one major change, *i.e.* the slow motion of the purine around the glycosidic angle χ. Here, we can confidently attribute a WC ↔ HG equilibrium to the three successive A·T base pairs composing the $T_6A_7A_8{\cdot}T_{17}T_{18}A_{19}$ segment. It should be underlined that the HG percentages calculated here for A_7, A_8 and A_{19} are among the highest measured populations[15,17–20].

In addition to the purine rotation, the WC → HG transition is accompanied by some changes in sugar pucker and backbone torsion angles, which likely optimize hydrogen-bonding and stacking with neighbours[19,27,42]. In particular, a study of either WC or HG A·T containing oligomers showed that ^{31}P signals are up-field shifted in and around HG A·T base pairs compared to their WC counterparts[42]. Such shifts are usually interpreted as being due to the presence of more BI conformers[47,48].

Examining high-resolution X-ray structures of free DNA suggests that another backbone alteration could also occur on α/γ angles, as briefly previously mentioned[27]. Indeed, structures containing exclusively HG pairings (PDB codes 1GQU and 1RSB, of 2.5 and 2.2 Å of resolution, respectively) enclose TpA junctions adopting unusual α/γ:g+/g− angles, instead of the canonical g-/g+ configuration. Unusual α/γ angles are infrequent in WC B-DNA X-ray structures[49,50] because they are energetically very costly to generate[50]. Nevertheless, as rare as they are, these atypical α/γ conformations are mainly encountered in ApA steps or A·T-rich contexts (Supplementary Table S4). So, the potential ability of A·T-rich patches to adopt unusual α/γ conformations could be a factor promoting the emergence of HG base pairs.

Sequence effect on TpA steps. The results presented above demonstrate that adenine H2 resonances associated with linewidth broadenings reflect the existence of a slow conformational exchange, as previously postulated[7,9,10]. However, any adenine submitted to slow motions is not associated with such anomalies that exclusively arise on TpA adenines. Accordingly, H2 linewidth broadenings are observed in the dodecamer on only those adenines belonging to TpA, A_7 and A_{19} (Fig. 1). This specific phenomenon may be related to the especially high-field shifted H2 resonance of the major conformer (Fig. 1) that likely maximizes Δω, and consequently R_{ex}—recalling that a high R_{ex} broadens the resonance.

This intimate connection between H2 linewidth broadening and slow motion allows the re-examination of earlier NMR data. A study reported measurements of H2 linewidth broadenings on 14 oligomers containing the 16 possible immediate sequence contexts of TpA steps (*i.e.* NTAN)[7,8]. This systematic approach showed that broadening of H2 occurs in diverse TpA environments, the maximal values corresponding to the central adenines of (Y/R)TAA tetramer fragments (Table 6).

However, considering the nearest neighbour is insufficient to explain the slight but significant disparity of H2 linewidth broadenings of the TpA adenines that are in the same tetrameric environment in CTTTAAATTTAAAG[8] and GCTTAATTAAGC[7] (Table 6). Similarly, H2 broadening (Fig. 1) and slow motion characteristics differ between A_7 and A_{19} in $TTA_7AA{\cdot}TTA_{19}A$, for instance the population of the excited state (p_E) (Table 2). These differences suggest a subtle, long-range influence of the sequence on the DNA's ability to undergo WC ↔ HG transitions. At this stage, the only certitude is that slow DNA motions are modulated at dinucleotide and tetranucleotide levels, as previously established in solution for nano-second dynamics[37,47,51].

References	Oligomer sequence	A in TpA with max H2 linewidth > 15 Hz
McAteer et al. 1995	CTTT**A**^{1}AATTT**A**^{2}AAG	TT**A**^{1}A (~ 15 Hz) and TT**A**^{2}A (~ 19 Hz)
	CTTTACATGT**A**AAG	GT**A**A
	CTTTAGATCT**A**AAG	CT**A**A
	CTTTATATAT**A**AAG	AT**A**A
McAteer et al. 2000	GCTTATAT**A**AGC	AT**A**A
	GCATACGT**A**TGC	GT**A**T
	GCTTAGCT**A**AGC	CT**A**A
	GCTT**A**^{1}ATT**A**^{2}AGC	TT**A**^{1}A (~ 18 Hz) and TT**A**^{2}A (~ 22 Hz)
	GCTTACGT**A**AGC	GT**A**A

Table 6. TpA steps associated with large H2 linewidth broadenings in the literature. This table reports the sequences studied by Kennedy's group in which the H2 linewidth broadening of one or two adenines (in bold, underlined) in TpA steps is equal or exceeds 15 Hz at 25 °C. The immediate environment of such TpA is reported in the last column. Note that all sequences are palindromic.

Discussion

This NMR study focused on a dodecamer containing the TTAAA·TTTAA fragment that was assumed to be an element facilitating histone anchoring upon nucleosome formation[34–37]. Slow conformational exchanges in the dodecamer were revealed and characterized from $R_{1\rho}$ relaxation dispersion experiments. These NMR approaches also allowed a re-examination of classical 1D and 1D-T1 inversion-recovery experiments and to demonstrate the relationship between H2 linewidth broadenings and slow motions. Given that linewidth is easily observable and quantifiable, it represents an interesting means of detecting nucleotide slow dynamics, even if it appears to be limited to TpA adenine H2 protons.

As expected, most nucleotides of the dodecamer do not show consistent, conclusive signs of any slow motion. However, A_7, A_8, and A_{19} in the $TA_7A_8{\cdot}TTA_{19}$ fragment are specifically subjected to conformational exchange in the milli-second time range. The corresponding exchange parameters perfectly match the signature of WC↔HG base pair equilibrium as published by Al-Hashimi's group[15,17–20]. Thus, we can confidently postulate that the $TA_7A_8{\cdot}TTA_{19}$ fragment is composed of three base pairs that transiently flip toward the HG conformation.

Although the crystallographic form of the ATTAAT·ATTAAT hexamer[52] attests for the co-existence of three or more successive HG base pairs, our analyses agree with non-simultaneous WC↔HG transitions of the three A·T base pairs, which does not exclude a certain degree of cooperation between the motions. For instance, that one HG base pair locally destabilizes the double helix[42] could favour a WC→HG flip of its closest neighbours. In any case, individual motions have the effect of magnifying the time during which one HG base pair is present in the TAA·TTA tract. Thus, according to the individual HG populations calculated here (~ 1% for each of the three HG base pairs), and given the non-simultaneous character of the motions highlighted by our fits, 3% of TAA·TTA fragment contains one HG A·T base pair.

This relatively high occurrence underlines the relevance of the question of an eventual function of transient HG base pairs in the nucleosome context, remembering that the TTAAA element likely helps histone anchoring. The first idea is that DNA wrapping could involve HG base pairs but our analyses failed to detect such pairing in high-resolution X-ray nucleosome structures, conversely to what was observed on several other types of DNA–protein complexes[27]. Another proposal relates to the exploitation of shape features specific to HG base pairs upon nucleosome formation. To our knowledge, there is only one structure ensemble based on NMR data that was collected on an oligomer containing one HG $m^1A{\cdot}T$ base pair in the $Am^1ACC{\cdot}GGTT$ environment[42]. This oligomer has as a main characteristic a major-groove kink. Indeed, analyses of X-ray structures of DNA bound to proteins or small molecules suggested that such major-groove curvature is induced by any HG base pair in any context[27,42]. This structural particularity cannot be considered as a favourable pre-organization for the nucleosome since TTAAA bound to the histone octamer presents a minor groove curvature[34,53]. In addition to the determination of the structure of our HG oligomer itself, another factor such as long-range consequence of HG base pair could be investigated. It has to be borne in mind that, at this point in time, there is no clear indication of how those HG base pairs present in the TAA element impact on nucleosome structure or dynamics. Indeed, it is now widely accepted that nucleosome assembly is primarily modulated by sequences that introduce structural variability for helical parameters such as roll or slide along the free WC B-DNA.

The percentage of HG conformers of the three A·T base pairs in $T_6A_7A_8{\cdot}T_{17}T_{18}A_{19}$ is unusually high (~ 1%) for such minor, short-lived states that very rarely exceed 0.5%[15,17–20]. Multiple examples of enhanced dynamics on TA·TA adenines in the same TAA·TTA context emerge when one considers studies reporting linewidth broadenings (Table 4)[7,8]. However, the structural foundation for this specific, sequence dependent, stabilisation of HG base pairs remains unclear and poorly documented. One can only formulate hypotheses, being aware that such speculations will require future investigation. A first point concerns atypical features observed in A·T containing sequences. Thus, the photo reactivities of TT steps in TTAA·TTAA leading to T^T dimers are clearly outsized compared to those of any other dinucleotides, comprising other TT steps[53]; this particularity is added to (but cannot be totally explained by) the TTAA·TTAA marked positive rolls and low twists attested by both NMR[37,54] and simulation[55] data. Also, as highlighted in one of the above sections, A·T rich sequences show a specific propensity to adopt unusual α/γ backbone angle conformations (Supplementary Table S4). Such unusual structural

elements could destabilize the WC form of A·T, favour the flipping-out of adenine from the double helix via the major groove[15,56], which preludes WC↔HG conversions, and, in the case of α/γ angles, stabilize the HG base pair. Another suggestion emerges from the X-ray structure of the DNA bound to the MATα2 homeodomain[57]. In this complex, the $T_6A_7A_8{\cdot}T_{36}T_{37}A_{38}$ fragment contains one HG base pair, $A_7{\cdot}T_{37}$, in which A_7 engages two hydrogen bonds with T_{37} and T_{36}. A similar way to increase the stability of HG conformers may occur in any TAA·TTA fragment, in the present case via hydrogen bonds between A_7A_8 and $T_{16}T_{17}T_{18}$ on the one hand and between A_{19} and T_5T_6 on the other.

Indeed, the effect of sequence in WC↔HG transition whilst incontestable remains complex and thus so far is only partially elucidated as already noted[17]. Further investigations are clearly required to clarify in particular, the effect of the tetra or even hexanucleotide contexts on the HG population. This topic is in fact essential for capturing the multiple aspects of DNA double helix functional versatility. A lot of information about nanosecond dynamics keeping WC pairing intact is already available; these are primarily sensitive to the dinucleotide sequence while modulated at the tetramer level, as shown by experimental X-ray[49,58,59] or NMR data[47,48,51,54] and modelling[38,55,60]. NMR data in particular revealed that such rapid motions are especially enhanced in G·C rich elements[47,51,54]. Several examples demonstrated their importance in the structural adjustment of DNA to its protein partners, transcription factors[61–63] or other proteins[37,51,64]. Beyond what occurs on WC G·C rich sequences at short timescales, A·T rich elements could be more specialized in milli-second conformational transitions, with the possibility of generating regions of Hoogsteen base-pair hot-spots that could play a topological role in genomic DNA[27].

Materials and methods

Samples and resonance assignments. Samples were purchased as single-stranded oligonucleotides 5′-CCGCTTAAACGC-3′ and 5′-GCGTTTAAGCGG-3′ from Eurogentec (Belgium) for unlabelled DNAs or from Eurisotop (France) for fully $^{15}N/^{13}C$–labeled DNAs. The two complementary strands were resuspended in 66 mM sodium phosphate buffer with 0.1 mM EDTA, for a total ionic strength of 0.1 M at pH 6.5; they were then mixed with a 1:1 ratio in 450 µL H_2O. In a next step, the samples were lyophilized three times in 99.99% ^2H_2O. The final concentration of the unlabelled and labelled duplexes were 1.2 mM and 0.85 mM respectively in volumes of 500 µL and 180 µL respectively.

The full assignment of ^1H and ^{13}C resonances of the dodecamer were previously described[37,54]. To complete the carbon assignments and notably to obtain those of the quaternary carbons of bases, we performed additional experiments on a Bruker Avance spectrometer equipped with a 5-mm triple-resonance cryogenic probe, at 600 MHz frequency or 150 MHz for ^{13}C experiments: (i) constant time ^1H-^{13}C HSQC optimized separately for aromatic and aliphatic carbons, C2 of adenine, C8 of purines, C5 and C6 of pyrimidines and C1′ of any base and, (ii) for the quaternary carbons C4, C5, C6 of adenines, 3D TROSY relayed HCCH-COSY[65] according to Hansen et al.[14].

$R_{1\rho}$ relaxation dispersion experiments. All experiments were performed on the same spectrometer as used for assignments, at pH 6.5 and 25 °C. As specified in the Results section, the linewidth broadening of H2-proton resonances is maximal at this temperature. 1D selective ^{13}C $R_{1\rho}$ pulse was applied as previously described[14,16]. The spin-lock powers (ω) needed to be carefully controlled, and were calibrated accordingly[14]. On-and off-resonance experiments were performed on C2, C6/C8 and C1′ atoms of the $^{13}C/^{15}N$-labeled DNA. On-resonance data were recorded at various ω, from ~ 100 to 3,500 Hz; off-resonance data were collected at various spin-lock offset frequencies (Ω) and at three or four different spin-lock powers (ω). Details of these experiments are given in Supplementary Table S1. Ten delays were used to determine T_{relax}, the monoexponential decrease of the magnetization: 0, 4, 8, 12, 12, 16, 20, 24, 32, 32 ms for C6, C8 and C2 carbons and 0, 4, 8, 12, 12, 18, 26, 34, 42 and 42 ms for C1′ carbons.

Note that the duplication of two delays in each experiment allowed an evaluation of errors in the measurement of the peak heights. These errors were subsequently used in Monte Carlo simulations to determine $R_{1\rho}$ uncertainties. The data corresponding to Hartmann-Hahn matching were omitted from the fits of on-and off-resonance measurements as previously described[14]. The 1D dispersion data were processed using NMRPipe[66].

Equilibrium parameters from $R_{1\rho}$ relaxation dispersion experiments. Our approach assumed a two–state equilibrium between a ground state G and a minor, excited state E in which p_G and p_E, the G and E populations, are strongly asymmetric: $pG \gg pE$. The equilibrium parameters that can be extracted from relaxation dispersion experiments are pG, pE, k_{ex} the exchange rate, $\Delta\omega_{GE}$ the difference between the frequencies of G and E, and R_{ex}, the quantity added to the relaxation rate due to exchange, which depends on p_G, p_E, k_{ex} and $\Delta\omega_{GE}$.

On-resonance experiments. R_{ex} was obtained by fitting the profiles of data from on-resonance experiments carried out in function of spin-lock offset powers (ω). In these experiments, θ, the angle between the effective field and the z axis, has the particular value of π/2. The fit is based on Eq. (1), a version of Eq. (2) that is simplified by using θ = π/2 to represent the condition of on-resonance experiments. For each fit, 500 runs were performed using $R_{1\rho}$ values.

$$R_{1\rho} = R_2 + R_{ex} = R_2 + \frac{\Phi_{ex} k_{ex}}{\omega_1^2 + k_{ex}^2}; \quad \Phi_{ex} = p_G p_E \Delta\omega_{GE}^2 \tag{1}$$

R_1 and R_2 are the intrinsic longitudinal and transverse relaxation rates, respectively, which are supposed to be identical for the two-states G and E; ω_1 is the spin-lock power.

Off-resonance experiments. The profiles of the off-resonance relaxation dispersion data measured in function of spin-lock offset frequencies (Ω) and power (ω) were fitted by two methods described below.

Method 1 is based on the Eq. (2)[15,43–45].

$$R_{1\rho} = R_1 \cos^2\theta + R_2 \sin^2\theta + \sin^2\theta \frac{p_G p_E \Delta\omega_{GE}^2 k_{ex}}{\Omega_E^2 + \omega_1^2 + k_{ex}^2} \quad (2)$$

In this case, restraints were applied on R_2: $R_2 \geq 16\ s^{-1}$ and $R_2 \leq 19\ s^{-1}$, according to the range inferred from on-resonance experiments; Ω_E and Ω_G are the resonance offsets for the excited and the ground states E and G, respectively; $\Delta\omega_{GE} = \Omega_E - \Omega_G$;

ω_1 is the spin-lock power related to by the relation

$$\tan\theta = \omega_1 / \Omega_{ave},\ \text{with}\ \Omega_{ave} = \Omega_E p_E + \Omega_G p_G\ \text{and}\ \ p_E + p_G = 1.$$

$k_{ex} = k_G + k_E$ is the exchange rate with $k_G = p_E k_{ex}$ and $k_E = p_G k_{ex}$, k_G and k_E representing the forward and reverse rate constants, respectively.

For each fit, 1000 runs were performed using $R_{1\rho}$ values. The $R_{1\rho}$ values from off-resonance experiments were systematically and randomly varied using standard deviations derived from the fits of the exponentially decreasing intensities of the peaks as function of the relaxation time. This protocol implemented using home-based Python and R scripts enables to derive the errors associated to each exchange parameter according to a strategy described previously[67].

Method 2 used the "Bloch-McConnell Numerical Simulator" (BMNS) developed by Al-Hashimi's group[3], which is exclusively based on a two-state exchange model. The calculations were performed with the same constraints on the R_2 relaxation rates than for the fits described above.

Received: 28 August 2020; Accepted: 12 October 2020
Published online: 04 November 2020

References

1. Mittermaier, A. K. & Kay, L. E. Observing biological dynamics at atomic resolution using NMR. *Trends Biochem. Sci.* **34**, 601–611 (2009).
2. Palmer, A. G. Chemical exchange in biomacromolecules: past, present, and future. *J. Magn. Reson.* **241**, 3–17 (2014).
3. Rangadurai, A., Szymaski, E. S., Kimsey, I. J., Shi, H. & Al-Hashimi, H. M. Characterizing micro-to-millisecond chemical exchange in nucleic acids using off-resonance R1ρ relaxation dispersion. *Prog. Nucl. Magn. Reson. Spectrosc.* **112–113**, 55–102 (2019).
4. Walinda, E., Morimoto, D. & Sugase, K. Overview of relaxation dispersion NMR spectroscopy to study protein dynamics and protein-ligand interactions. *Curr. Protoc. Protein Sci.* **92**, e57 (2018).
5. Lefevre, J. F., Lane, A. N. & Jardetzky, O. A temperature dependent transition in the Pribnow box of the trp promoter. *FEBS Lett.* **190**, 37–40 (1985).
6. Lefevre, J. F., Lane, A. N. & Jardetzky, O. A description of conformational transitions in the Pribnow box of the trp promoter of *Escherichia coli*. *Biochemistry* **27**, 1086–1094 (1988).
7. McAteer, K. & Kennedy, M. A. NMR evidence for base dynamics at all TpA steps in DNA. *J. Biomol. Struct. Dyn.* **17**, 1001–1009 (2000).
8. McAteer, K., Ellis, P. D. & Kennedy, M. A. The effects of sequence context on base dynamics at TpA steps in DNA studied by NMR. *Nucleic Acids Res.* **23**, 3962–3966 (1995).
9. Kennedy, M. A., Nuutero, S. T., Davis, J. T., Drobny, G. P. & Reid, B. R. Mobility at the TpA cleavage site in the T3A3-containing AhaIII and PmeI restriction sequences. *Biochemistry* **32**, 8022–8035 (1993).
10. Lingbeck, J. *et al.* Effect of adenine methylation on the structure and dynamics of TpA steps in DNA: NMR structure determination of [d(CGAGGTTTAAACCTCG)]2 and its A9-methylated derivative at 750 MHz. *Biochemistry* **35**, 719–734 (1996).
11. Palmer, A. G. Enzyme dynamics from NMR spectroscopy. *Acc. Chem. Res.* **48**, 457–465 (2015).
12. Baronti, L. *et al.* Base-pair conformational switch modulates miR-34a targeting of Sirt1 mRNA. *Nature* **583**, 139–144 (2020).
13. Bothe, J. R. *et al.* Characterizing RNA dynamics at atomic resolution using solution-state NMR spectroscopy. *Nat. Methods* **8**, 919–931 (2011).
14. Hansen, A. L., Nikolova, E. N., Casiano-Negroni, A. & Al-Hashimi, H. M. Extending the range of microsecond-to-millisecond chemical exchange detected in labeled and unlabeled nucleic acids by selective carbon R(1rho) NMR spectroscopy. *J. Am. Chem. Soc.* **131**, 3818–3819 (2009).
15. Nikolova, E. N. *et al.* Transient Hoogsteen base pairs in canonical duplex DNA. *Nature* **470**, 498–502 (2011).
16. Xue, Y. *et al.* Characterizing RNA excited states using NMR relaxation dispersion. *Meth. Enzymol.* **558**, 39–73 (2015).
17. Alvey, H. S., Gottardo, F. L., Nikolova, E. N. & Al-Hashimi, H. M. Widespread transient Hoogsteen base pairs in canonical duplex DNA with variable energetics. *Nat Commun* **5**, 4786 (2014).
18. Nikolova, E. N., Gottardo, F. L. & Al-Hashimi, H. M. Probing transient Hoogsteen hydrogen bonds in canonical duplex DNA using NMR relaxation dispersion and single-atom substitution. *J. Am. Chem. Soc.* **134**, 3667–3670 (2012).
19. Shi, H. *et al.* Atomic structures of excited state A-T Hoogsteen base pairs in duplex DNA by combining NMR relaxation dispersion, mutagenesis, and chemical shift calculations. *J. Biomol. NMR* **70**, 229–244 (2018).
20. Xu, Y., McSally, J., Andricioaei, I. & Al-Hashimi, H. M. Modulation of Hoogsteen dynamics on DNA recognition. *Nat. Commun.* **9**, 1473 (2018).
21. Abrescia, N. G. A., Thompson, A., Huynh-Dinh, T. & Subirana, J. A. Crystal structure of an antiparallel DNA fragment with Hoogsteen base pairing. *Proc. Natl. Acad. Sci. USA* **99**, 2806–2811 (2002).
22. Abrescia, N. G. A., González, C., Gouyette, C. & Subirana, J. A. X-ray and NMR studies of the DNA oligomer d(ATATAT): Hoogsteen base pairing in duplex DNA. *Biochemistry* **43**, 4092–4100 (2004).
23. Cubero, E., Abrescia, N. G. A., Subirana, J. A., Luque, F. J. & Orozco, M. Theoretical study of a new DNA structure: the antiparallel Hoogsteen duplex. *J. Am. Chem. Soc.* **125**, 14603–14612 (2003).
24. Singh, U. C., Pattabiraman, N., Langridge, R. & Kollman, P. A. Molecular mechanical studies of d(CGTACG)2: complex of triostin A with the middle A–T base pairs in either Hoogsteen or Watson-Crick pairing. *Proc. Natl. Acad. Sci. U.S.A.* **83**, 6402–6406 (1986).
25. Chakraborty, D. & Wales, D. J. Energy Landscape and Pathways for Transitions between Watson-Crick and Hoogsteen Base Pairing in DNA. *J Phys Chem Lett* **9**, 229–241 (2018).

26. Cubero, E., Luque, F. J. & Orozco, M. Theoretical study of the Hoogsteen-Watson-Crick junctions in DNA. *Biophys. J.* **90**, 1000–1008 (2006).
27. Zhou, H. *et al.* New insights into Hoogsteen base pairs in DNA duplexes from a structure-based survey. *Nucleic Acids Res.* **43**, 3420–3433 (2015).
28. Brogaard, K., Xi, L., Wang, J.-P. & Widom, J. A map of nucleosome positions in yeast at base-pair resolution. *Nature* **486**, 496–501 (2012).
29. Langley, S. A., Karpen, G. H. & Langley, C. H. Nucleosomes shape DNA polymorphism and divergence. *PLoS Genet.* **10**, e1004457 (2014).
30. Lieleg, C., Krietenstein, N., Walker, M. & Korber, P. Nucleosome positioning in yeasts: methods, maps, and mechanisms. *Chromosoma* **124**, 131–151 (2015).
31. Nalabothula, N. *et al.* Archaeal nucleosome positioning in vivo and in vitro is directed by primary sequence motifs. *BMC Genom.* **14**, 391 (2013).
32. Struhl, K. & Segal, E. Determinants of nucleosome positioning. *Nat. Struct. Mol. Biol.* **20**, 267–273 (2013).
33. Thåström, A., Bingham, L. M. & Widom, J. Nucleosomal locations of dominant DNA sequence motifs for histone-DNA interactions and nucleosome positioning. *J. Mol. Biol.* **338**, 695–709 (2004).
34. Chua, E. Y. D., Vasudevan, D., Davey, G. E., Wu, B. & Davey, C. A. The mechanics behind DNA sequence-dependent properties of the nucleosome. *Nucleic Acids Res.* **40**, 6338–6352 (2012).
35. Elbahnsi, A., Retureau, R., Baaden, M., Hartmann, B. & Oguey, C. Holding the nucleosome together: a quantitative description of the DNA-histone interface in Solution. *J. Chem. Theory Comput.* **14**, 1045–1058 (2018).
36. Wu, B., Mohideen, K., Vasudevan, D. & Davey, C. A. Structural insight into the sequence dependence of nucleosome positioning. *Structure* **18**, 528–536 (2010).
37. Xu, X. *et al.* NMR studies of DNA support the role of pre-existing minor groove variations in nucleosome indirect readout. *Biochemistry* **53**, 5601–5612 (2014).
38. Ben Imeddourene, A. *et al.* Simulations meet experiment to reveal new insights into DNA intrinsic mechanics. *PLoS Comput. Biol.* **11**, e1004631 (2015).
39. Rohs, R., West, S. M., Liu, P. & Honig, B. Nuance in the double-helix and its role in protein-DNA recognition. *Curr. Opin. Struct. Biol.* **19**, 171–177 (2009).
40. Wijmenga, S. S., Kruithof, M. & Hilbers, C. W. Analysis of (1)H chemical shifts in DNA: Assessment of the reliability of (1)H chemical shift calculations for use in structure refinement. *J. Biomol. NMR* **10**, 337–350 (1997).
41. Palmer, A. G. NMR characterization of the dynamics of biomacromolecules. *Chem. Rev.* **104**, 3623–3640 (2004).
42. Sathyamoorthy, B. *et al.* Insights into Watson-Crick/Hoogsteen breathing dynamics and damage repair from the solution structure and dynamic ensemble of DNA duplexes containing m1A. *Nucleic Acids Res.* **45**, 5586–5601 (2017).
43. Korzhnev, D. M., Orekhov, V. Y. & Kay, L. E. Off-resonance R(1rho) NMR studies of exchange dynamics in proteins with low spin-lock fields: an application to a Fyn SH3 domain. *J. Am. Chem. Soc.* **127**, 713–721 (2005).
44. Palmer, A. G. & Massi, F. Characterization of the dynamics of biomacromolecules using rotating-frame spin relaxation NMR spectroscopy. *Chem. Rev.* **106**, 1700–1719 (2006).
45. Trott, O. & Palmer, A. G. R1rho relaxation outside of the fast-exchange limit. *J. Magn. Reson.* **154**, 157–160 (2002).
46. Dethoff, E. A., Chugh, J., Mustoe, A. M. & Al-Hashimi, H. M. Functional complexity and regulation through RNA dynamics. *Nature* **482**, 322–330 (2012).
47. Heddi, B., Foloppe, N., Bouchemal, N., Hantz, E. & Hartmann, B. Quantification of DNA BI/BII backbone states in solution. Implications for DNA overall structure and recognition. *J. Am. Chem. Soc.* **128**, 9170–9177 (2006).
48. Tian, Y. *et al.* 31P NMR investigation of backbone dynamics in DNA binding sites. *J. Phys. Chem. B* **113**, 2596–2603 (2009).
49. Djuranovic, D. & Hartmann, B. Conformational characteristics and correlations in crystal structures of nucleic acid oligonucleotides: evidence for sub-states. *J. Biomol. Struct. Dyn.* **20**, 771–788 (2003).
50. Várnai, P., Djuranovic, D., Lavery, R. & Hartmann, B. Alpha/gamma transitions in the B-DNA backbone. *Nucleic Acids Res.* **30**, 5398–5406 (2002).
51. Heddi, B., Oguey, C., Lavelle, C., Foloppe, N. & Hartmann, B. Intrinsic flexibility of B-DNA: the experimental TRX scale. *Nucleic Acids Res.* **38**, 1034–1047 (2010).
52. Acosta-Reyes, F. J., Alechaga, E., Subirana, J. A. & Campos, J. L. Structure of the DNA duplex d(ATTAAT)2 with Hoogsteen hydrogen bonds. *PLoS ONE* **10**, e0120241 (2015).
53. Hatakeyama, A., Hartmann, B., Travers, A., Nogues, C. & Buckle, M. High-resolution biophysical analysis of the dynamics of nucleosome formation. *Sci. Rep.* **6**, 27337 (2016).
54. Imeddourene, A. B. *et al.* The intrinsic mechanics of B-DNA in solution characterized by NMR. *Nucleic Acids Res.* **44**, 3432–3447 (2016).
55. Dans, P. D. *et al.* The static and dynamic structural heterogeneities of B-DNA: extending Calladine-Dickerson rules. *Nucleic Acids Res.* https://doi.org/10.1093/nar/gkz905 (2019).
56. Lindahl, V., Villa, A. & Hess, B. Sequence dependency of canonical base pair opening in the DNA double helix. *PLoS Comput. Biol.* **13**, e1005463 (2017).
57. Aishima, J. *et al.* A Hoogsteen base pair embedded in undistorted B-DNA. *Nucleic Acids Res.* **30**, 5244–5252 (2002).
58. Djuranovic, D. & Hartmann, B. DNA fine structure and dynamics in crystals and in solution: the impact of BI/BII backbone conformations. *Biopolymers* **73**, 356–368 (2004).
59. Schneider, B. *et al.* A DNA structural alphabet provides new insight into DNA flexibility. *Acta Crystallogr D Struct Biol* **74**, 52–64 (2018).
60. Zgarbová, M. *et al.* Influence of BII backbone substates on DNA twist: a unified view and comparison of simulation and experiment for all 136 distinct tetranucleotide sequences. *J. Chem. Inf. Model* **57**, 275–287 (2017).
61. Djuranovic, D., Oguey, C. & Hartmann, B. The role of DNA structure and dynamics in the recognition of bovine papillomavirus E2 protein target sequences. *J. Mol. Biol.* **339**, 785–796 (2004).
62. Heddi, B., Foloppe, N., Oguey, C. & Hartmann, B. Importance of accurate DNA structures in solution: the Jun-Fos model. *J. Mol. Biol.* **382**, 956–970 (2008).
63. Tisné, C., Delepierre, M. & Hartmann, B. How NF-kappaB can be attracted by its cognate DNA. *J. Mol. Biol.* **293**, 139–150 (1999).
64. Heddi, B., Abi-Ghanem, J., Lavigne, M. & Hartmann, B. Sequence-dependent DNA flexibility mediates DNase I cleavage. *J. Mol. Biol.* **395**, 123–133 (2010).
65. Simon, B., Zanier, K. & Sattler, M. A TROSY relayed HCCH-COSY experiment for correlating adenine H2/H8 resonances in uniformly 13C-labeled RNA molecules. *J. Biomol. NMR* **20**, 173–176 (2001).
66. Delaglio, F. *et al.* NMRPipe: a multidimensional spectral processing system based on UNIX pipes. *J. Biomol. NMR* **6**, 277–293 (1995).
67. Bothe, J. R., Stein, Z. W. & Al-Hashimi, H. M. Evaluating the uncertainty in exchange parameters determined from off-resonance R1ρ relaxation dispersion for systems in fast exchange. *J. Magn. Reson.* **244**, 18–29 (2014).

Acknowledgements
Dr Al-Hashimi and Dr Kimsey are warmly thanked for having helped in the development of dispersion relaxation methods in our laboratory. The authors also thank the NMR team in Gif/Yvette, in particular Carine van Heijenoort and Nelly Morellet, for instructive discussions.

Author contributions
A.B.I. and L.Z. performed the NMR experiments under the supervision of O.M., the leader project. A.B.I. and O.M. carried out most analyses and wrote the original draft. A.B.I., O.M. and B.H. prepared all the figures. B.H. participated to some analyses and wrote the final manuscript with M.B. All authors reviewed the manuscript.

Competing interests
The authors declare no competing interests.

Additional information
Supplementary information is available for this paper at https://doi.org/10.1038/s41598-020-75645-x.

Correspondence and requests for materials should be addressed to O.M.

Reprints and permissions information is available at www.nature.com/reprints.

Publisher's note Springer Nature remains neutral with regard to jurisdictional claims in published maps and institutional affiliations.

Open Access This article is licensed under a Creative Commons Attribution 4.0 International License, which permits use, sharing, adaptation, distribution and reproduction in any medium or format, as long as you give appropriate credit to the original author(s) and the source, provide a link to the Creative Commons licence, and indicate if changes were made. The images or other third party material in this article are included in the article's Creative Commons licence, unless indicated otherwise in a credit line to the material. If material is not included in the article's Creative Commons licence and your intended use is not permitted by statutory regulation or exceeds the permitted use, you will need to obtain permission directly from the copyright holder. To view a copy of this licence, visit http://creativecommons.org/licenses/by/4.0/.

© The Author(s) 2020